International Journal of Pharmaceutics 617 (2022) 121632

Contents lists available at ScienceDirect

International Journal of Pharmaceutics

journal homepage: www.elsevier.com/locate/ijpharm

Carbamazepine polymorphism: A re-visitation using Raman imaging

Sara Fateixa *, Helena I.S. Nogueira, Tito Trindade

Department of Chemistry and CICECO-Aveiro Institute of Materials, University of Aveiro, 3810-193 Aveiro, Portugal

ARTICLE INFO

Keywords:
Confocal Raman microscopy
Raman imaging
Carbamazepine
Polymorphism
Cluster analysis
Thermal methods

ABSTRACT

Raman imaging methods have appeared in the last years as a powerful approach to monitoring the quality of pharmaceutical compounds. Because polymorphism occurs in many crystalline pharmaceutical compounds, it is essential to monitor polymorphic transformations induced by different external stimulus, such as temperature changes, to which those compounds may be submitted. Raman imaging with k-means cluster analysis (CA) is used here as an essential technique to investigate structural and chemical transformations occurring in carbamazepine p-monoclinic (CBZ **III**) into carbamazepine triclinic (CBZ **I**) when submitted to temperatures near the melting point of CBZ **III** (178 °C) and CBZ **I** (193 °C).

CBZ **III** commercial powder and laboratorial prepared CBZ **I** were analyzed by differential scanning calorimetry, powder X-ray diffraction and Raman spectroscopy with variable temperature. After thermal treatment, the resultant CBZ powder was evaluated by Raman imaging, in which all imaging data was analyzed using CA. Raman imaging allowed the identification of different polymorphs of CBZ (CBZ **III** and CBZ **I**) and iminostilbene (IMS), a degradation product of CBZ, in the treated samples, depending on the heating treatment method.

1. Introduction

Polymorphism is the ability of a compound to crystalize into distinct crystalline forms depending on the ambient and experimental conditions. Monitoring and controlling the polymorphism behavior of molecular compounds have been a long-standing challenge in various applications. In particular, polymorphs of pharmaceutical compounds have distinct physical–chemical properties that impact their bioavailability and chemical stability.(Censi and Di Martino, 2015; Diao et al., 2012; Hilfiker, 2006; Hilfiker and Raumer, 2019; Rodríguez-Spong et al., 2004) The European Pharmacopeia has shown that 57% of pharmaceutical compounds are capable of forming hydrates, 20% form solvates, and about 58% are polymorphic.(Bechtloff et al., 2001)

Carbamazepine (CBZ, 5*H*-dibenzazepine-5-carboxamide) is an anticonvulsant drug belonging to the Biopharmaceutics Classification System II Class, which is used to treat epilepsy and to relieve trigeminal neuralgia.(Dołęga et al., 2019; Flicker et al., 2011; O'Brien et al., 2004)

There are five anhydrous polymorphic forms reported in the literature, though the terminology to distinguish the several forms lacks uniformity, with some authors using a Roman numerical system and others using a Greek notation. Here, the CBZ polymorphs are named according to the terminology followed by Grzesiak *et al.*(Grzesiak et al., 2003) and F. Flicker *et al.* (Flicker et al., 2012, 2011) as follows: crystal lattice ρ-monoclinic (**III**), triclinic (**I**), c-monoclinic (**IV**), trigonal (**II**), a catemeric polymorph (**V**) and one dihydrate form.(Arlin et al., 2011; Grzesiak et al., 2003; Li et al., 2008) The polymorph CBZ **III** is the commercially available therapeutic agent and the thermodynamic stable form at room temperature.

Carbamazepine polymorphs and the hydrate compound have different dissolution rates in the human gastrointestinal tract, resulting in distinct bio-availability. Thus, depending on the pharmaceutical product history, different commercial brands of CBZ tablets can present distinct drug performances or even clinical failure due to CBZ polymorphism.(Meyer et al., 1992) This highlights the relevance of understanding and monitoring the polymorphism in CBZ products.

Carbamazepine presents a rare case of packing polymorphism, in which all four polymorphs (**I**, **II**, **III** and **IV**) present an identical molecular conformation (with differences in the packing of the carboxamide dimer units) and strong hydrogen bonding.(Grzesiak et al., 2003; Lang et al., 2002; Rodríguez-Spong et al., 2004) For instance, the CBZ polymorphs (**I** to **II**) pack in a similar mode, in which both modifications show two C-H•••O intermolecular interactions between an oxygen and two different hydrogen donors.(Rodríguez-Spong et al., 2004) The most recently discovered form **V** is the only known polymorph of CBZ that occurs in a catemeric configuration without forming dimers.(Arlin et al., 2011; Clout et al., 2018)

* Corresponding author.
E-mail address: sarafateixa@ua.pt (S. Fateixa).

https://doi.org/10.1016/j.ijpharm.2022.121632
Received 29 October 2021; Received in revised form 25 February 2022; Accepted 28 February 2022
Available online 2 March 2022

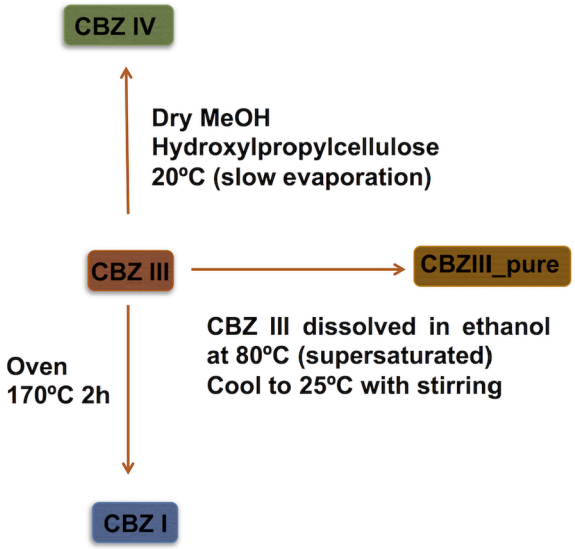

Scheme 1. Flow chart showing the preparation methods and thermal transition between CBZ polymorphs **I**, **III** and **IV**.

Spectroscopic techniques such as infrared (IR) and Raman spectroscopies have been widely used as characterization tools of Active Pharmaceutical Ingredients (APIs), namely in identifying polymorphs, co-crystals, impurities, amorphous materials and solvates.(Nanubolu and Burley, 2012) These vibrational spectroscopy techniques offer short periods of analysis time, involve non-contact and non-destructive measurements, fast sample preparation and, in the case of Raman measurements, the samples can be measured directly in water without solvent interference.(Inoue et al., 2019; Kogermann et al., 2007; Tian et al., 2006) Although both techniques probe molecular vibrations and are frequently employed as complementary tools, Raman spectroscopy presents more sensitivity for APIs detection (stronger Raman signal) than for the excipients commonly used. This is because Raman spectroscopy is not sensitive to high dipole moment bonds present in most excipients; however, it is highly sensitive to conjugated double bonds and aromatic rings that normally exist in a variety of APIs.(Farias and Carneiro, 2014) Consequently, Raman spectroscopy can detect changes in intramolecular bonding (e.g. C-C symmetric vibrations) and, as a result, reveal structural information at the molecular level.(Kogermann et al., 2007) Also, low-frequency Raman spectroscopy can be especially useful because it can easily differentiate API crystalline forms due to distinct lattice vibrational modes.(Inoue et al., 2017; Larkin et al., 2014; Roy et al., 2013; Taylor and Zografi, 1998) The last decade has assisted to an increasing interest in applying Raman imaging techniques to the development, manufacturing and quality control of pharmaceutical products.(Firkala et al., 2013; Nanubolu and Burley, 2012; Piqueras et al., 2014) A main advantage of Raman based images is that they combine spatial and spectral information about the analyzed sample. A selected area of the sample is analyzed, with high spatial resolution (within the micrometer range), which allows to monitor the analyte even at low concentrations.(Fateixa et al., 2018a; Fateixa et al., 2018b; Mitsutake et al., 2019) Raman imaging has been used as an effective spectroscopic technique in the pharmaceutical field for the study of pharmaceutical formulations concerning drug/excipient distribution, particle/domain size and shape, crystallization and aggregation stage, phase separation, surface migration and polymorphic forms.(Brown et al., 2010; Carruthers et al., 2021; Clarke et al., 2001; Dadou et al., 2020; Di Febo et al., 2020; Sarri et al., 2019; Xu et al., 2020)

We have been exploring Raman imaging as a tool to characterize the distribution/aggregation state of specific compounds that are dispersed in composites, which in some cases have great interest for pharmaceutical areas, namely in drug delivery, cancer therapies and bone regeneration.(Fateixa et al., 2017; Marques et al., 2019; Monteiro et al., 2018)

Raman imaging is particularly suitable to study polymorphic transformations due to the significant differences in the Raman features of the

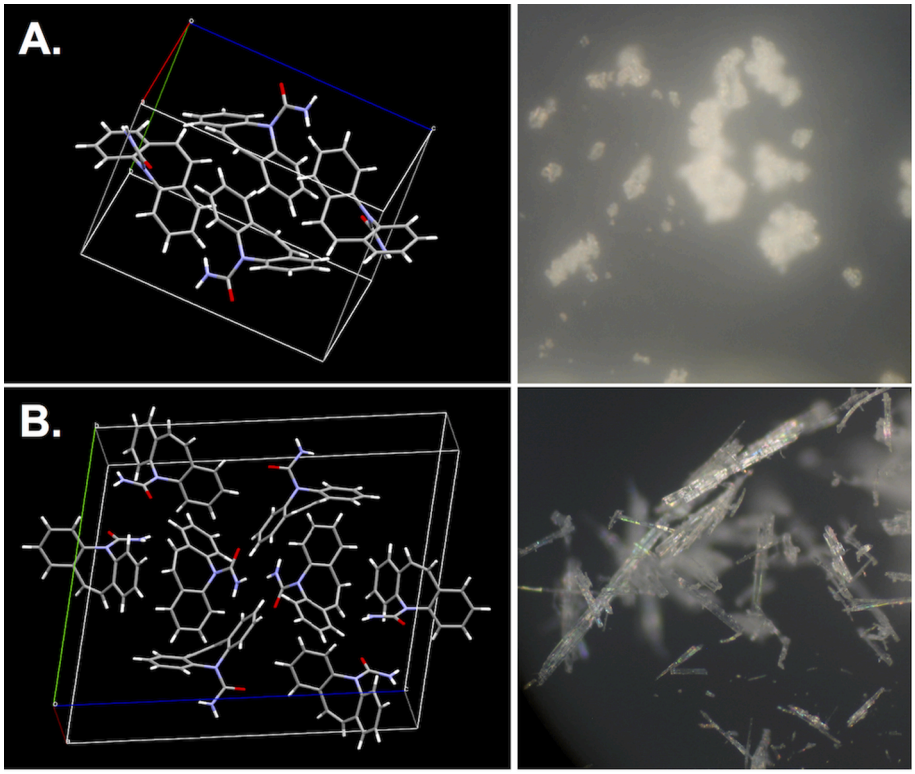

Fig. 1. Molecular packing (left) and optical microscope image (right, 10x objective) of (A) CBZ ρ-monoclinic (CBZ **III**), (B) CBZ triclinic (CBZ **I**). The molecular packing of CBZ polymorphs was performed using the program Mercury 4.1 and the data retrieved from WebCSD.

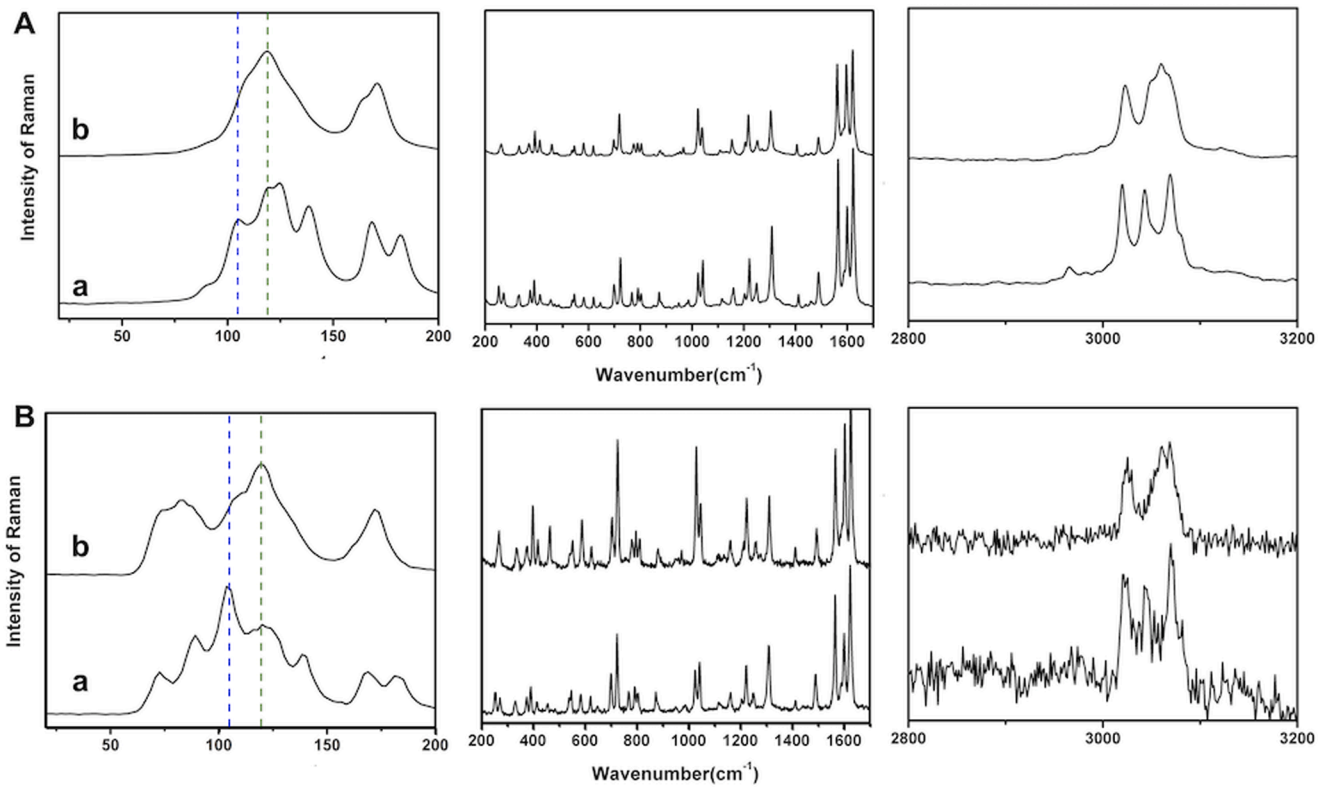

Fig. 2. Raman spectra of CBZ **III (a)** and CBZ **I (b)**, using two different laser sources 1064 nm (A) and 633 nm (B). The three panels correspond to different spectral regions. Dashed lines highlight the diagnosis bands chosen to monitor the presence of CBZ **III** (blue dashed line; 104 cm^{-1}) and CBZ **I** (green dashed line; 118 cm^{-1}). (For interpretation of the references to colour in this figure legend, the reader is referred to the web version of this article.)

polymorphs, allowing their detection in different areas of the sample. (Clout et al., 2018; Di Febo et al., 2020; Piqueras et al., 2014; Sarri et al., 2019) For instance, Piqueras *et al.* have reported the use of multiset analysis on several Raman images acquired during the thermal-induced polymorphic transformation of CBZ, providing a complete description of this process from global (image) and local (pixel) level and structural (identification of the polymorphic forms) point of view.(Piqueras et al., 2014) They have proven the presence of two CBZ polymorphs forms (ρ-monoclinic (**III**) and an unidentified CBZ polymorph) at the beginning of the thermal degradation process (25 °C) of anhydrous commercial CBZ, using fixed-size image window-evolving factor analysis (FSIW-EFA). Both CBZ polymorphs have evolved to a third one (CBZ **I**) after exposure to a gradient temperature until they reach 160 °C. Burley and co-workers have used in situ Raman spectroscopy and Raman imaging to monitor the crystallization behavior of amorphous paracetamol for variable temperatures in both covered and uncovered sample holders.(Nanubolu and Burley, 2012) Using this imaging technique, they have demonstrated that amorphous paracetamol samples synthesized under variable experimental conditions can exhibit differences in the crystallization pathway.

Although the characterization of the different CBZ polymorphs and the associated transformation conditions have been reported, an updated overall picture of the CBZ polymorphism process is important. Namely, there is a lack of detailed investigation on the temperature influence in CBZ polymorphs crystal structure and degradation products. The transition of CBZ III into CBZ I during heating has been investigated using a variety of techniques such as DSC analysis, Raman and IR spectroscopies and powder X-ray diffraction;(Behme and Brooke, 1991; Edwards et al., 2001; Flicker et al., 2012; Hu et al., 2019a; O'Brien et al., 2004; Piqueras et al., 2014; Rustichelli et al., 2000a) however, the polymorphism process of CBZ during the cooling step and re-heating has been less studied. Recently, Dołęga *et al.* have shown that the temperature of CBZ decomposition is lower than the melting point of CBZ I (~192 °C), and identified the presence of iminostilbene (IMS) during the re-heating of CBZ **III** sample using DSC analysis and powder X-ray diffraction.(Dołęga et al., 2020b, 2020a, 2019)

Hence, this research aims to provide a systematic overview of carbamazepine ρ-monoclinic (CBZ **III**) crystallization into carbamazepine triclinic (CBZ **I**) under different experimental and analytical conditions using confocal Raman microscopy. In particular, this work reports for the first time Raman imaging, together with k-means cluster analysis (CA), to identify the polymorphic transition of CBZ **III** into CBZ **I** and the degradation product of CBZ **III** (iminostilbene). Furthermore, the spatial distribution of CBZ **III** (API) in commercial tablets is also reported here by using the Raman imaging technique, demonstrating the potential of this approach for quality monitoring purposes.

2. Experimental section

2.1. Materials

Carbamazepine polymorph **III** powder (CBZ **III**) was purchased from Sigma-Aldrich (St. Louis, MO, USA) and used as received; hydroxypropyl cellulose (M_w = 60000, Sigma-Aldrich). All solvents were obtained from commercial sources and used as received or distilled and dried by standard procedures. Safety: CBZ is an API that should be handled in small amounts and under adequate safety conditions due to its toxicity. Waste from these compounds should be placed in containers for further treatment and disposal.

2.2. Preparation of CBZ polymorphs

Pure polymorph **III** (CBZ **III**_pure) was obtained by the dissolution of commercial CBZ **III** in ethanol (5.1 g/100 mL) at 80 °C, over 40 min, and then, the solution was cooled to 25 °C and held at this temperature for 5 h. The crystals obtained were filtered and dried overnight at 30 °C,

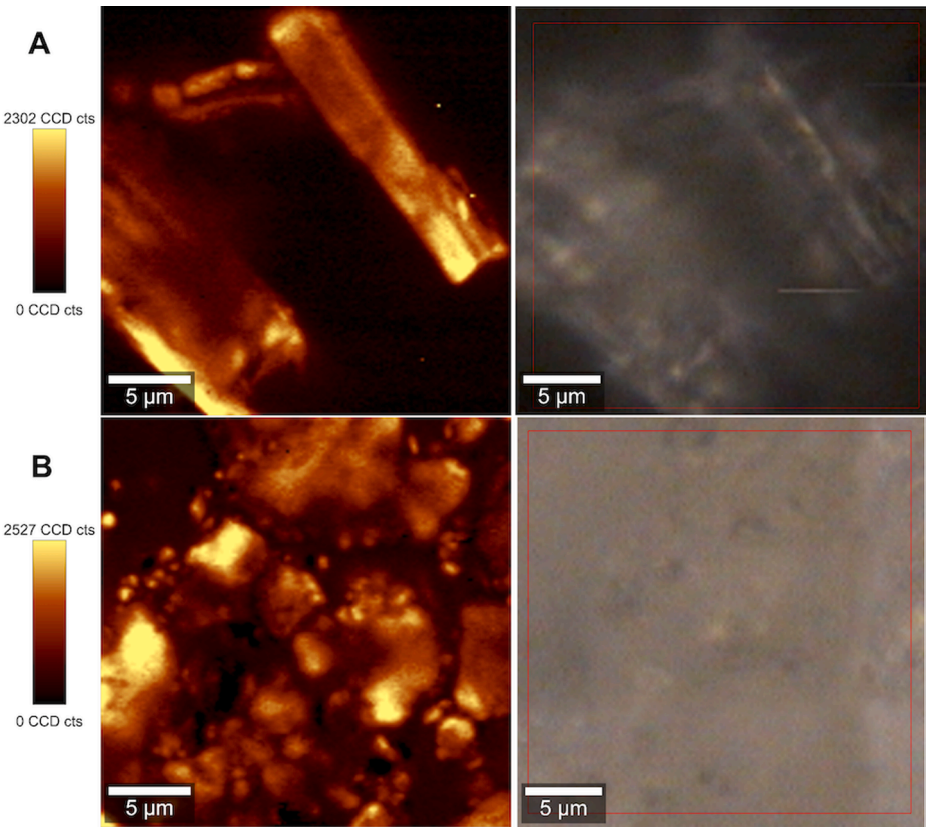

Fig. 3. Optical microscope images with the scanned area marked in red (right) and the respective Raman images (left, excitation at 633 nm) obtained using the integrated intensity of the Raman band at 118 cm^{-1} for CBZ **I** (A) and Raman band at 104 cm^{-1} for CBZ **III** (B). The vertical bar shows the color profile in the image with the relative intensity scale.

following the procedure of Li *et al.*(Li et al., 2008) CBZ polymorph I (CBZ **I**) was prepared by heating CBZ **III** at 170 °C for 2 h, as described previously by Strachan *et al.*(Strachan et al., 2004b) The CBZ polymorph IV (CBZ **IV**) was prepared by the slow evaporation of 0.6 mL of anhydrous methanol solution (1.5 g/100 mL, 20 °C) of CBZ **III** in the presence of 24 mg of hydroxypropyl cellulose, following the work of Lang *et al.*(Lang et al., 2002)

Scheme 1 summarizes a CBZ polymorphism flow chart, showing the preparation methods used in this paper and/or the thermal transitions between CBZ **I–IV**.

2.3. Temperature-dependent powder X-ray diffraction (XRD) analysis

Variable-temperature powder XRD studies were acquired at a heating rate of 5 °C/min. Pellets of CBZ polymorphs (~100 mg) with a diameter of 2.5 cm were placed in the cavity of a stainless-steel holder. The sample was first heated from 25 °C to 178 (or 195 °C) at 5 °C/min, held for 5 min at 178 °C (or 195 °C), and then left to cool down at room temperature (25 °C) on air. After the analysis, the room was ventilated to dispose of possible toxic products from the decomposition of CBZ.

2.4. Differential scanning calorimetry (DSC) measurements

The crystallization and melting dynamics of CBZ polymorphs were evaluated by DSC. For each sample, 2 cycles of heating–cooling were performed. In detail, the DSC analysis was carried out at a heating rate of 5 °C/min under N_2 atmosphere and in the temperature range of 25 °C to 195 °C. The sample was first heated from 25 °C to 195 °C, at 5 °C/min, held for 1 min at 195 °C and then cooled from 195 °C to 25 °C, at 5 °C/min, hold for 1 min at 25 °C and a second heating–cooling cycle was done immediately after, using the same instrumental parameters. The onset of each thermal event (T_{onset}) and the enthalpy (ΔH) were used to compare the endothermic and exothermic peaks of the CBZ sample.

2.5. FT-Raman measurements

FT-Raman spectra of CBZ **I** and CBZ **III** were measured using a FT-Raman spectrometer Bruker RFS 100/S with a laser excitation source at 1064 nm. Each Raman spectra were acquired with 200 scans, at a power of 100 mW and 4 cm^{-1} of resolution.

2.6. Temperature-dependent confocal Raman microscopy

A combined Raman-AFM-SNOM confocal microscope system WITec alpha300 RAS^{+} was used. Raman spectra of the CBZ polymorphs were acquired at 10mW of power, 10 acquisition, 2 s each acquisition using a 633 nm excitation laser source. Raman imaging was performed by taking 150 × 150 Raman spectra in a uniform 25 × 25 μm grid for small areas and 250 × 250 Raman spectra in a 100 × 100 μm grid for large areas. A 100 × objective was used, and the integration time for each spectrum was 0.05 s (power set at 10 mW). The time required to create the Raman images using that integration time was 22 min (small areas) and 60 min (large areas). CBZ tablets (400 mg of CBZ) were obtained from a commercial supplier; it was designed as CBZ-tablet. Raman imaging was performed on the commercial tablets by taking 600 × 300 Raman spectra in a uniform 6000 μm × 3000 μm grid with a 10x 0bjective (10 mW; 180,000 Raman spectra with 0.05 s and 1 acquisition each; 8 h) and Raman spectra were acquired on crushed CBZ-tablet (2 s, 10 acquisitions each).

Data acquisition and processing were performed using WITec Project 5.0^{+} software. The average Raman spectra were obtained from all data points in the Raman images (22500 spectra for small images; 62,500

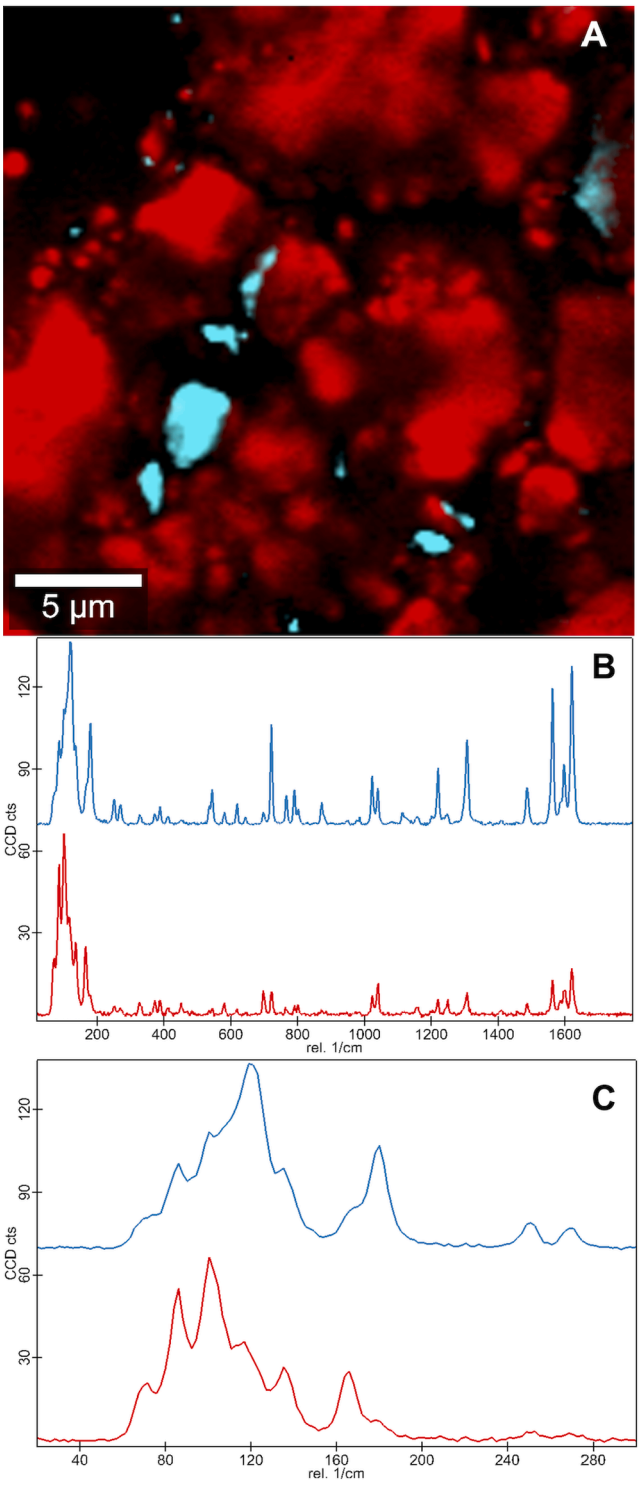

Fig. 4. Combined set of the Raman images obtained from the two different spectra observed in CBZ **III** using CA (A); corresponding average spectrum for each distinguished area (red and cyan, respectively) at the range 20–1800 cm^{-1} (B) and at low-frequency region (20–300 cm^{-1}) (C).

spectra for large areas). Raman images were constructed by area integrating over specific Raman bands of CBZ powders.

Background subtraction was performed for all Raman spectra and images, using the shape function (shape size: 300; noise factor: 2) of the Graph Background subtraction (WITec Project 5.0^{+}). All imaging data were analyzed using the k-means cluster analysis (CA) to distinguish different CBZ polymorphs and degradation products. Briefly, CA allows

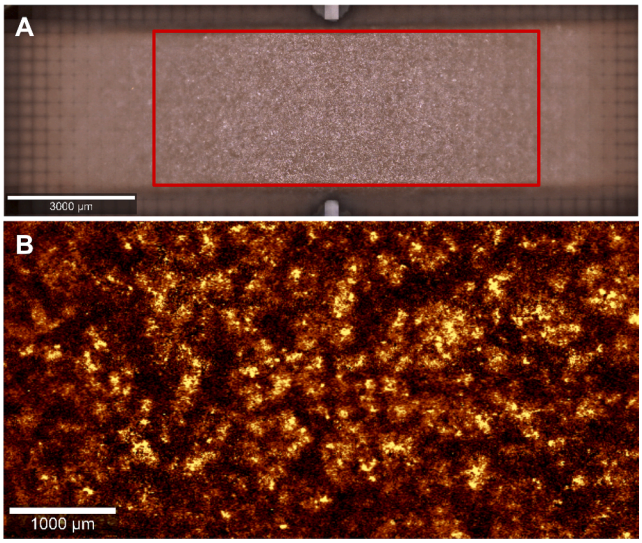

Fig. 5. A) Optical images of commercial CBZ-tablet with the scan area marked at red; B) Raman image obtained using the integrated intensity of the Raman band at 1624 cm^{-1} for CBZ **III**. (For interpretation of the references to colour in this figure legend, the reader is referred to the web version of this article.)

for grouping a set of objects (vibrational spectra in our studies) similar to each other (in vibrational features). CA was performed using WITec Project Plus software with the Centroid model and the k-means algorithm (a single mean vector represented each cluster). The hyperspectral image is processed into different color-coded images, representing the chemically different areas (clusters) and the corresponding average spectrum for each distinguished area. One cluster was assigned to CBZ **III** (red), CBZ **I** (blue) and iminostilbene (green). A combined image is used to represent the obtained clusters images.

The temperature-dependent Raman measurements were carried out at a heating rate of 5 °C/min from 25 to 178 °C or 193 °C (leaving 5 min at this temperature) and then return to room temperature (25 °C, without controlling the cooling step). Pellets of CBZ polymorphs (~10 mg) with a diameter of 1 cm were used, mounted between glass slides.

2.7. Instrumentation

Optical microscopy characterization was performed using a Carl Zeiss Axiovert 40 MAT microscope (Carl Zeiss Light Microscopy, Göttingen, Germany). The samples were prepared by direct deposition of the CBZ powder on glass slides. XRD was performed using a Philips instrument operating with Cu-Kα radiation (λ = 1.54060 Å) at 40 kV/50 mA. DSC analysis was carried out using a Power Compensation Diamond DSC – Perkin Elmer instrument calibrated between −90 °C and 500 °C, using In and Pb standards and hermetically sealed Al pans. The HPLC system comprised a column Kromasil 100–5-C18 (250 mm of length and 4.6 mm of i.d.) coupled to a precolumn holder (imChem). The column was maintained at 25 °C, and the mobile phase consisted of acetic acid 0.1% (35%) and methanol (65%) (isocratic elution) with a flow rate of 1 mL/min. The injection volume was 20 μL. The total run time was 45 min. Chromatographic standards of CBZ and IMS were used. The retention time (t_R) of CBZ was 6.5 min, whereas t_R of IMS was ca. 18 min. Both CBZ and IMS were detected at a wavelength of 260 nm.

3. Results

3.1. Optical microscopy

The two CBZ polymorphs used in this research work, namely CBZ commercial (CBZ **III**) and prepared CBZ **I**, can be clearly distinguished under the experimental conditions employed for this study. Fig. 1 (on

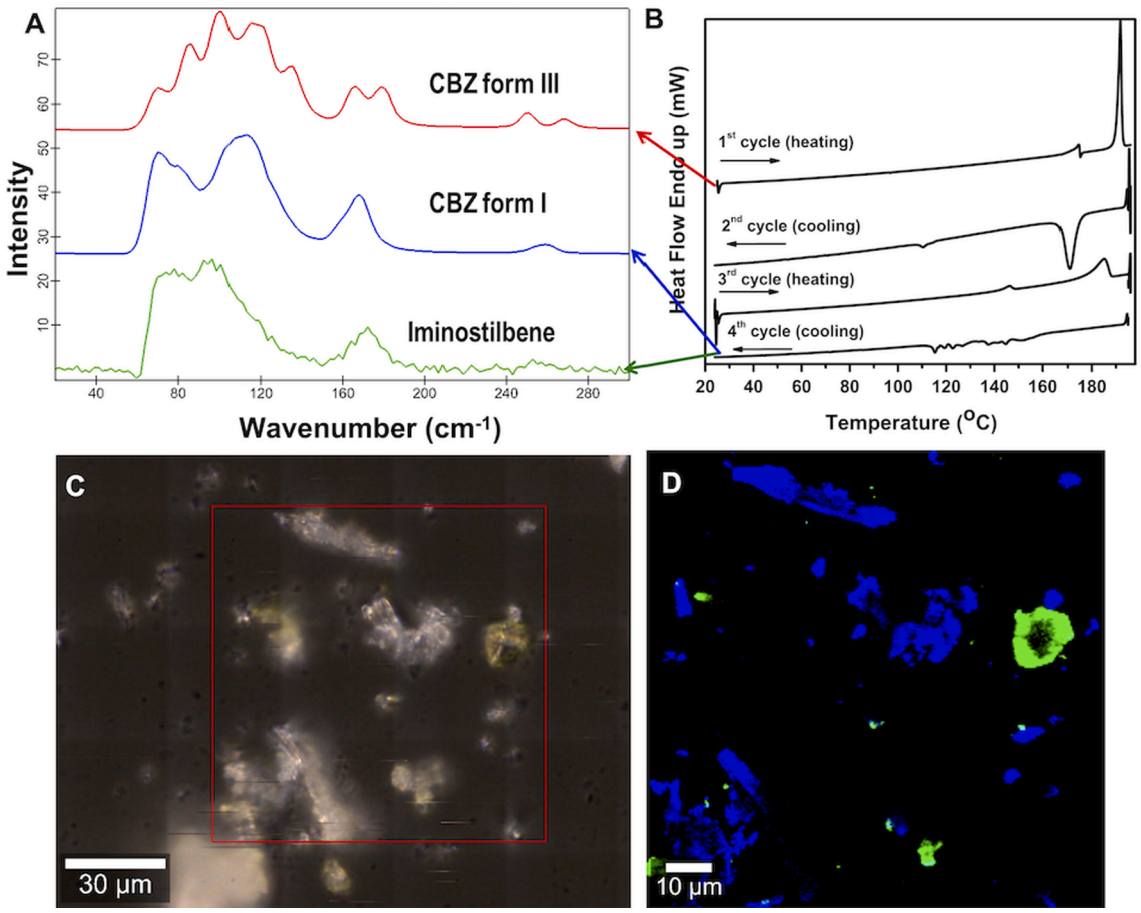

Fig. 6. A) Raman spectra of CBZ **III** powder before and after DSC heating–cooling experiments. B) DSC profile of CBZ **III**, using successive heating and cooling cycles. C) Optical microscope image of the powder after the heating–cooling experiments, with the Raman scanned area marked in red. D) Combined set of the Raman images (scanned area shown in C) obtained from the two different Raman spectra detected in the final powder using CA (green and blue colors in the image D and respective spectra in A). (For interpretation of the references to colour in this figure legend, the reader is referred to the web version of this article.)

the right) presents optical images of CBZ **III** and CBZ **I** using an optical microscope with polarized light. Both can be distinguished by simple visual inspection, having CBZ **III** crystals a prismatic-shape and CBZ **I** a large needle-shape. The molecular packing of carbamazepine in polymorphs CBZ **III** and CBZ **I** is also presented in Fig. 1 (on the left), showing the formation of dimers, with the carboxamide unit acting as both the hydrogen bond donor and acceptor.(Grzesiak et al., 2003)

3.2. FT-Raman and confocal Raman microscopy analysis

First, the two CBZ polymorph samples were analyzed by Raman spectroscopy using two distinct laser sources with excitation wavelength at 633 nm and 1064 nm.

The Raman spectra of CBZ **III** and CBZ **I** (Fig. 2) are in good agreement with those published in the literature,(Inoue et al., 2019; O'Brien et al., 2004; Rocha and Poppi, 2011; Strachan et al., 2004a) exhibiting the characteristic band positions and relative intensities of the ρ -monoclinic and triclinic forms, respectively. The Raman bands for both CBZ polymorphs have been assigned to the respective vibrational modes according to the literature,(O'Brien et al., 2004; Prasad et al., 2020; Rocha and Poppi, 2011; Tommasini et al., 2019) and are summarized in Table S1.

The two CBZ samples exhibit differences in the band positions and relative intensities of the Raman bands in the spectral regions of 1500–1600 cm^{-1} (stretching C═C modes of the aromatic rings), 1000–1100 cm^{-1} (bending in-plane mode of C—H from the aromatic rings) and 3040–3065 cm^{-1} (stretching mode of C—H in the aromatic rings).(O'Brien et al., 2004) Although the Raman spectra of two CBZ polymorphs present significant differences in these regions, no isolated distinct bands were found to monitor the two polymorphs, making its use challenging to identify the CBZ polymorphs in mixture samples.

The vibrational modes observed in the low-frequency region (20–200 cm^{-1}) in Fig. 2 (on the left) are due to the deformations of the molecular skeleton within the crystal lattice.(Inoue et al., 2019, 2017) CBZ exhibits several low-frequency Raman bands with high intensities (*e.g.* at 104 cm^{-1} for CBZ **III** and at 118 cm^{-1} for CBZ **I**) due to changes in the σ-π back-bonding between the primary amide and the aryl groups. (Larkin et al., 2014) Thus, these bands are suitable as diagnosis bands for monitoring the two CBZ polymorphs in pharmaceutical products.

The CBZ **III** and CBZ **I** crystals were characterized using Raman imaging (Fig. 3). The Raman images were obtained using the bands at 104 cm^{-1} and 118 cm^{-1} for CBZ **III** and CBZ **I**, respectively. The brighter colors in the images indicate the presence of the respective CBZ polymorph. It should be noted that by using Raman imaging, the characteristic needle-shaped crystals of CBZ **I**'s and the prismatic-shaped CBZ **III**'s crystals can be clearly observed.

In order to identify adventitious contaminants or distinct CBZ polymorphs in each CBZ sample, a k-means cluster analysis (CA) was performed on the Raman spectral data acquired. The CA coupled with Raman imaging has been used as a multivariate analysis to investigate pharmaceutical formulations (Chemical Characterization of Pharmaceutical Samples by Confocal Raman Microscopy and Correlative Techniques, n.d.) and other type of samples such as organelles in cells and ceramics.(Li et al., 2019; Środek et al., 2018)

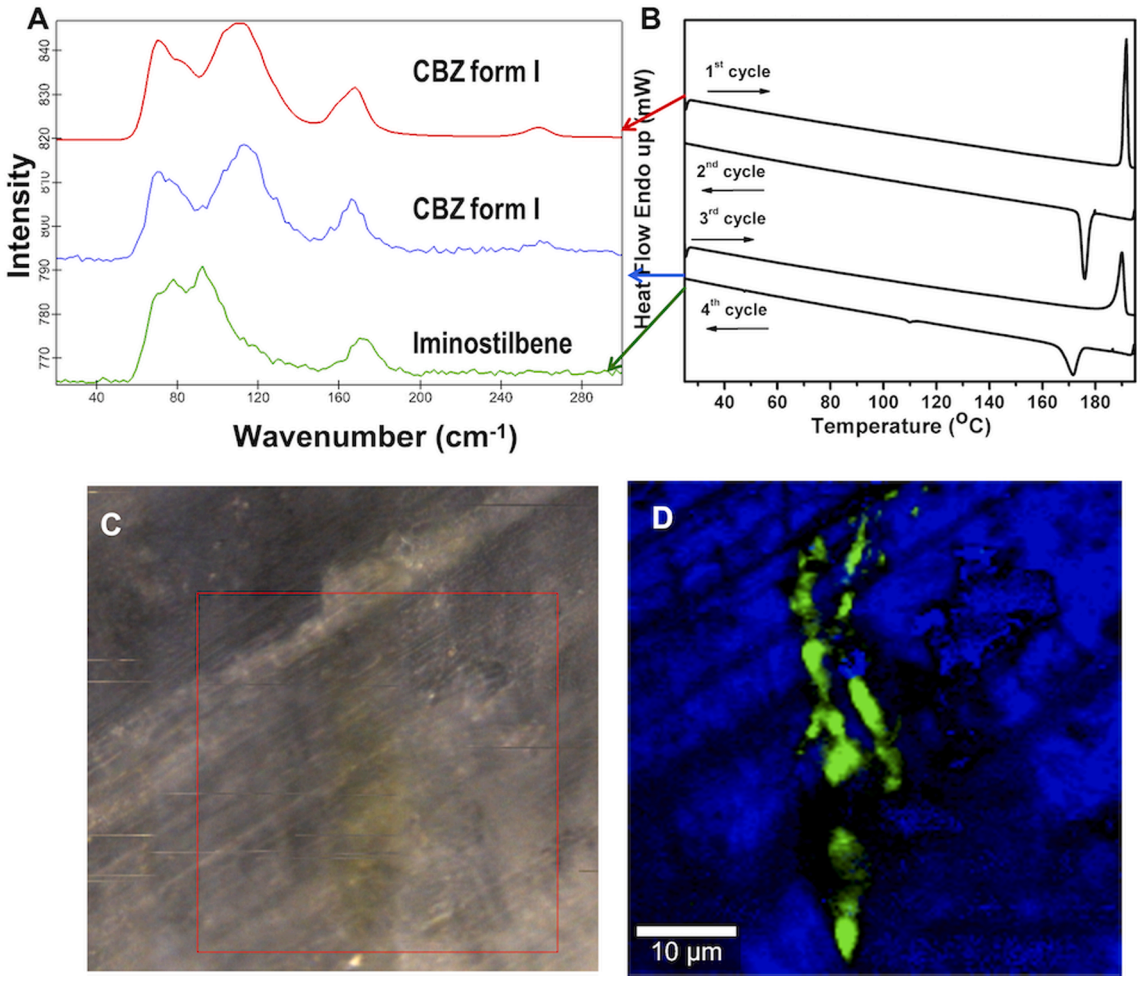

Fig. 7. A) Raman spectra of CBZ **I** powder before and after the two DSC heating–cooling experiments. B) DSC profile of CBZ **I**, using successive heating–cooling cycles. C) Optical microscope image of the powder after the heating–cooling experiments, with the Raman scanned area marked in red. D) Combined set of the Raman images (scanned area shown in C) obtained from the two different Raman spectra detected in the final powder using CA (green and blue colors in the image D and respective spectra in A). (For interpretation of the references to colour in this figure legend, the reader is referred to the web version of this article.)

In the Raman image of CBZ **I** powder, the characteristic Raman spectrum of CBZ **I** is observed over all regions of the needle-shaped crystals, indicating a complete transition of CBZ **III** to CBZ **I** (170 °C, 2 h). This means that no impurities, degradation products or CBZ **III** crystals have been observed in this sample.

The CA analysis on the Raman spectral data acquired for CBZ **III** (Fig. 4) allowed to detect the presence of a second Raman spectrum, similar to CBZ **III**, but with significant differences in band intensities (see top spectrum, cyan colored, in Fig. 4B). It should be noted the inversion of the band intensities at 1023 and 1041 cm^{-1}, assigned to the $\delta_{in\text{-}plane}$(C—H) aromatic and the increase of the Raman band intensities at 544 cm^{-1} assigned to the aromatic ring bending out-plane, 722 cm^{-1} assigned for the C—N—C stretching, 1223 cm^{-1} assigned to the C—H bending in-plane of the aromatic ring and 1307 cm^{-1} assigned to the C—H non-aromatic bending in-plane.(O'Brien et al., 2004)

Taking a careful inspection of both Raman spectra at lower wavenumbers (Fig. 4C), significant differences can be detected in the bands' intensities, namely 104 cm^{-1}, 120 cm^{-1}, 170 cm^{-1} and 181 cm^{-1}, all assigned to the lattice vibration of the CBZ **III** crystal; however, no changes on the band positions were observed.

Raman imaging was also used to investigate the distribution of the CBZ **III** over the surface of a commercial CBZ-tablet. In this case, the band at 1624 cm^{-1}, assigned to the ν(C═C) non-aromatic, was used for monitoring instead of the band at 104 cm^{-1}, as shown in Fig. 3. This is because the band at 143 cm^{-1}, due to TiO_2 used in the formulation, is very intense and difficult the monitoring of bands in that spectral region. The Raman image presented in Fig. 5 shows a homogeneous distribution of CBZ **III** at the surface of the tablet. Several Raman spectra were also acquired on crushed CBZ-tablet, and the characteristic Raman features for CBZ **III** can be clearly observed (Figure S2).

3.3. DCS measurements

Fig. 6 presents the DSC results for CBZ **III**, using successive heating–cooling cycles and the respective Raman spectra of the solid CBZ powder before and after the DSC analysis. Before heating the sample, a Raman image was recorded, from which an average Raman spectrum was obtained (Fig. 6A, red spectrum). In the first heating cycle (1st cycle in Fig. 6B), an endothermic peak immediately followed by an exothermic peak is observed at 174.5 °C (T_{onset} = 171.6 °C), corresponding to the melting of CBZ **III**, followed by crystallization into the CBZ form **I**. A second endothermic peak is observed at 193 °C, corresponding to the melting of CBZ **I**. During the first cooling step (2nd cycle in Fig. 6B), the recrystallization of the CBZ **I** occurs with the exothermic peak at 175.3 °C (T_{onset} = 178.2 °C). This result is in good agreement with thermal data reported in the literature.(Behme and Brooke, 1991; Dołęga et al., 2019; Grzesiak et al., 2003)

A second heating–cooling experiment (3rd and 4th cycles in Fig. 6B) was performed to investigate the presence of CBZ degradation products arising from thermal treatment. In the second heating cycle (3rd cycle in

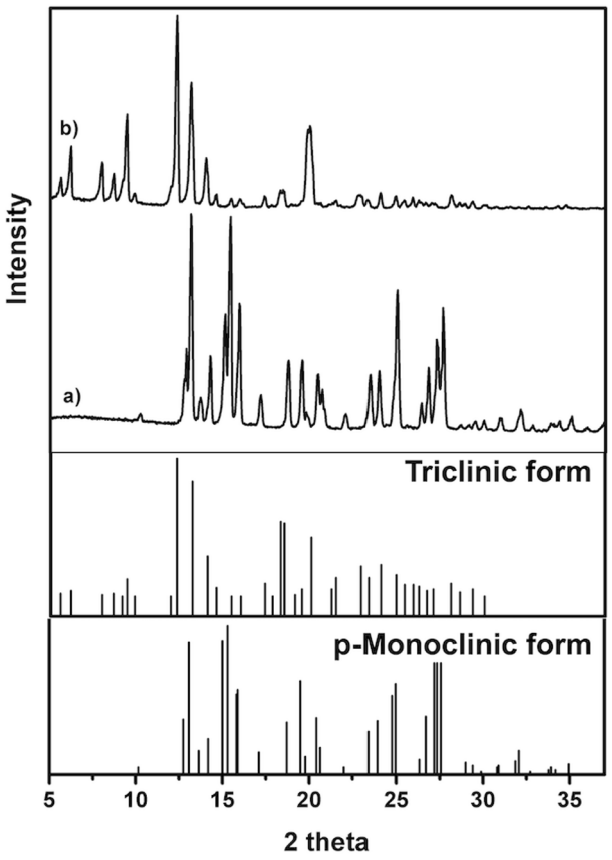

Fig. 8. Powder XRD diffraction patterns of samples CBZ **III** (a) and CBZ **I** (b). The bottom diffractograms correspond to the literature data for the CBZ polymorphs: ρ-monoclinic (JCPDS Card No. 00–033-1565) and triclinic (JCPDS Card No. 00–056-1968).

Fig. 6B), two endothermic peaks at 146.2 °C (T_{onset} = 142.5 °C) and 185.0 °C (T_{onset} = 177.6 °C) were observed. It has been reported that carbamazepine can sublime and condense as orange crystals of iminostilbene (IMS), when exposed to higher temperatures.(Ceolin et al., 1997) Dołęga et al. have observed the same thermal events for CBZ **III,** demonstrating that such endothermic peaks are due to the melting of IMS (146.2 °C) and CBZ **I** (185.0 °C), respectively. (Dołęga et al., 2020b, 2019) These authors have found the presence of IMS on the decomposition process of CBZ **III** even below the temperature reported as the melting point of CBZ **I** (225 °C).

The yellow powder obtained after the DSC analysis of CBZ **III** was characterized by Raman imaging. The CA of the Raman spectral data acquired shows the distribution of two distinct Raman spectra (Raman image in Fig. 6D, with colors corresponding to the spatial location of the blue and green spectra shown in Fig. 6A, respectively). According to the literature, the blue spectrum corresponds to CBZ **I** and the green spectrum corresponds to IMS (complete Raman spectrum of IMS shown in Figure S1).(Kuramshina et al., 2003) The combined Raman image shows the presence of CBZ **I** needle-shaped crystals and IMS particles, but the latter in less amount. This result was confirmed by HPLC, in which two peaks were observed for the yellow powder obtained after the DSC analysis (Figure S3). The first peak is related to CBZ (retention time 6.5 min), and the second peak is from IMS (retention time 18 min).

Similar heating–cooling experiments were performed with CBZ **I.** For CBZ **I,** an unique endothermic peak is observed at 191 °C (T_{onset} = 189.9 °C), correspondent to the melting of CBZ **I** in the first heating cycle (Fig. 7B).(Hu et al., 2019b; Rustichelli et al., 2000b) During the cooling step (2nd cycle in Fig. 7B), the recrystallization of the CBZ **I** is observed by the exothermic peak at 175.3 °C (T_{onset} = 178.2 °C). In the second cooling step (4th cycle in Fig. 7B), a shift for lower temperatures of the crystallization of CBZ **I** is detected. This could be an evidence for IMS formation.

The yellow powder obtained after the DSC analysis of CBZ **I** was characterized by Raman imaging (Fig. 7D). The presence in the sample of CBZ **I** crystals (blue) and IMS particles (green) were confirmed.

3.4. Temperature-dependent powder XRD diffraction

Fig. 8 shows the powder XRD for the two CBZ samples. The XRD diffractogram of CBZ **III** corresponds to the ρ-monoclinic form with space group P21/c and lattice parameters: a = 7.529, b = 11.148, c = 15.470, β = 116.17. The CBZ molecules pack as hydrogen bonded dimers through the carboxamide group with an anti (centrosymmetric) relationship (Fig. 1A). The main XRD peaks reported in the literature for the ρ-monoclinic CBZ are located at 2θ = 12.9, 14.9, 15.2, 15.8, 27.2, 27.5 and 32.0°.(Flicker et al., 2011; Grzesiak et al., 2003; Lang et al., 2002) At lower angles (5–20° 2θ), the powder XRD diffractogram shows slight differences in the peak intensities (14.9 and 18.0° 2θ) that can be due to different crystal habits, smaller particle size or preferred orientation of the particles in the sample holder.(Flicker et al., 2012, 2011) The CBZ **I** powder presents the expected lattice parameters for the triclinic lattice: a = 5.1706, b = 20.574, c = 22.245, α = 84.12, β = 88.01 and γ = 85.419 (Fig. 8b).(Ceolin et al., 1997; Grzesiak et al., 2003) The asymmetric unit consists of four molecules, each forming hydrogen-bonded *anti* dimers through the carboxamide donor and carbonyl acceptor (Fig. 1B).(Grzesiak et al., 2003) These results are in agreement with the results of the Raman spectroscopy presented above (Fig. 2).

To have further information about the thermal behavior of CBZ, the CBZ **III** powder was analyzed by temperature-dependent XRD, followed by Raman imaging of the final powder. Fig. 9A shows that a mixture of CBZ **III** and CBZ **I** is present in the sample at 178 °C, as revealed by the XRD patterns corresponding to both polymorphs. At this temperature, the characteristic XRD peaks of CBZ **I** (2θ 7–10° and 12.5°) are also observed in the heated CBZ **III** sample, which become more pronounced when the sample is cooled to room temperature (25 °C).

To have more information about the transition of CBZ **III** powder into CBZ **I** at 178 °C, a Raman image was recorded after the sample was cooled to room temperature. Fig. 9D shows a combined set of the Raman images (scanned area shown in Fig. 9C) obtained from the spatial distribution of the two different Raman spectra detected in the final powder (the corresponding spectra are shown in Fig. 9B, with the same colors). The combined Raman image of the sample (Fig. 9D), indicates the presence of a mixture of CBZ **III** (red) and CBZ **I** (blue), in which the latter predominates; the Raman data analysis also confirmed the absence of IMS in the thermal treated sample.

A temperature-dependent powder XRD characterization for CBZ **III** using an upper temperature near the melting point of CBZ **I** (193 °C) was also performed. In this case, the CBZ **III** was quantitatively converted into CBZ **I,** as shown in Figure S4. The Raman image of the final powder shows the presence of CBZ **I**, but no CBZ **III** or IMS were detected from the Raman data.

The CBZ **I** crystals were also analyzed by powder XRD using in situ temperature variation (Figure S5). For CBZ **I**, no changes were observed in the XRD patterns by increasing the temperature of the analyzed sample, and the observed Raman bands were characteristic of CBZ **I.**

3.5. Temperature-dependent Raman spectroscopy

This research clearly indicates the relevance of the thermal treatment to which the sample is submitted for the polymorphic transition/degradation of CBZ **III.** Thus, a temperature-dependent Raman spectroscopic study was carried out for the first time by submitting the sample to a temperature variation and recording the Raman spectra in situ. Fig. 10 indicates that the transition of CBZ **III** into CBZ **I** occurs at 160 °C, as revealed by the characteristic Raman bands of CBZ **I.** The

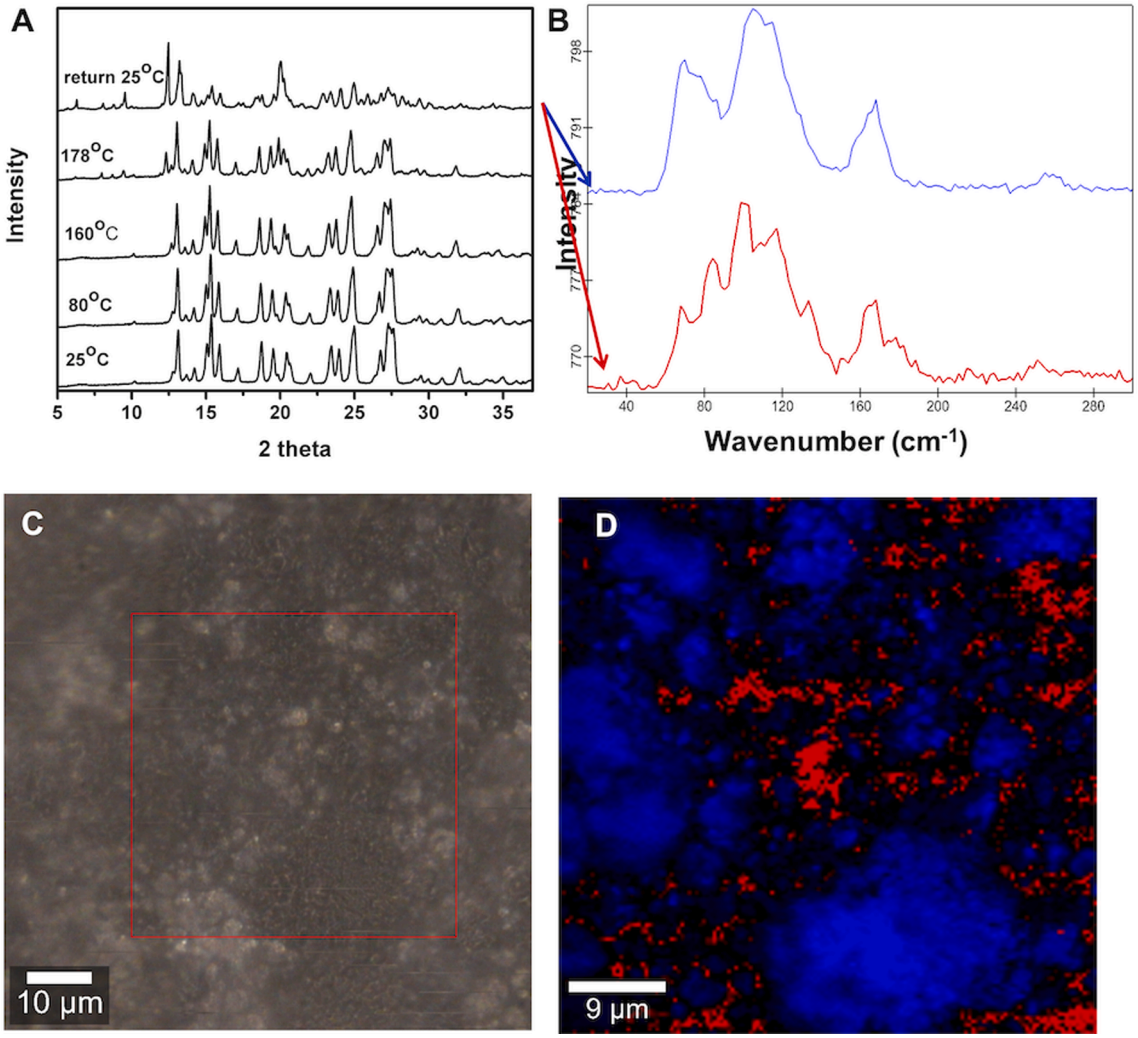

Fig. 9. A) XRD powder diffractograms of CBZ **III**, at several temperatures, during one heating–cooling cycle. B) Raman spectra obtained for CBZ **III** powder after being heated (up to 178 °C) and cooled to room temperature (CBZ **III** – red spectrum; CBZ **I** – blue spectrum). C) Optical microscope image of the powder after the heating–cooling experiments, with the Raman scanned area marked in red. D) Combined set of the Raman images (scanned area shown in C) obtained from the two different Raman spectra detected in the final powder using CA (red and blue colors in the image D and respective spectra in A). (For interpretation of the references to colour in this figure legend, the reader is referred to the web version of this article.)

spectra do not show the presence of degradation products (*e.g.* IMS). The Raman imaging in Fig. 10B was recorded on the powder sample after being cooled to room temperature. The Raman spectrum in Fig. 10A shows the characteristic Raman bands of CBZ **I** when the sample is cooled to room temperature, the Raman imaging after CA shows the presence of both IMS (green) and CBZ **I** (blue). The Raman imaging of a sample submitted to a similar treatment but up to 178 °C as the maximum temperature showed CBZ **I** needle-shape crystals as the single phase (See supporting information, Figure S6).

4. Discussion

This work confirms Raman imaging as a powerful tool to monitor polymorphic changes occurring in active pharmaceutical ingredients and identify compounds that might result from eventual degradation. All the characterization techniques used in this research show that CBZ **III** corresponds to the ρ-monoclinic form and CBZ **I** to the triclinic form. It is known that CBZ products exhibit a history of irregular drug performance and clinical failures on generic tablets or tablets of the same brand due to high dissolution variability.(Flicker et al., 2011; Kobayashi et al., 2000; Mittapalli et al., 2008) Following this line, CBZ polymorphs powders were analyzed by Raman imaging followed by k-means CA to identify possible degradation products or contamination compounds. For CBZ I, a quantitative conversion of CBZ **III** into CBZ **I** (needle-shaped particles) occurred at 170 ° after heating over 2 h, without observation of any byproduct, such as IMS (Fig. 3A). On the other hand, the Raman image acquired for CBZ **III** (Fig. 3B) has demonstrated the presence of CBZ **III** (cubic-shape particles) and another unidentified compound with a different Raman spectrum (Fig. 4, cyan Raman spectrum).

As a first hypothesis, it was thought that the Raman spectrum of the unknown compound could be attributed to vestigial IMS, which is used for the fabrication of CBZ **III**. A close comparison of the IMS Raman spectrum (Fig. 6, green Raman spectrum) with the one obtained in Fig. 4 (cyan Raman spectrum), it was concluded that the cyan Raman spectrum does not correspond to IMS.

Some authors have reported that commercial CBZ **III** can contain a minor amount of CBZ **IV.**(Flicker et al., 2011; Kipouros et al., 2005) In order to evaluate the presence of this polymorph in the CBZ **III** sample, CBZ **IV** was firstly prepared using the method described by Lang *et al.* (Lang et al., 2002) The powder XRD diffractogram and Raman spectrum revealed a crystalline phase belonging to the c-monoclinic system(Lang et al., 2002; Strachan et al., 2004b) (See supporting information, Figure S7). It turns out that the Raman spectrum of CBZ **IV** presented in Figure S7 did not match the cyan Raman spectrum presented in Fig. 4B.

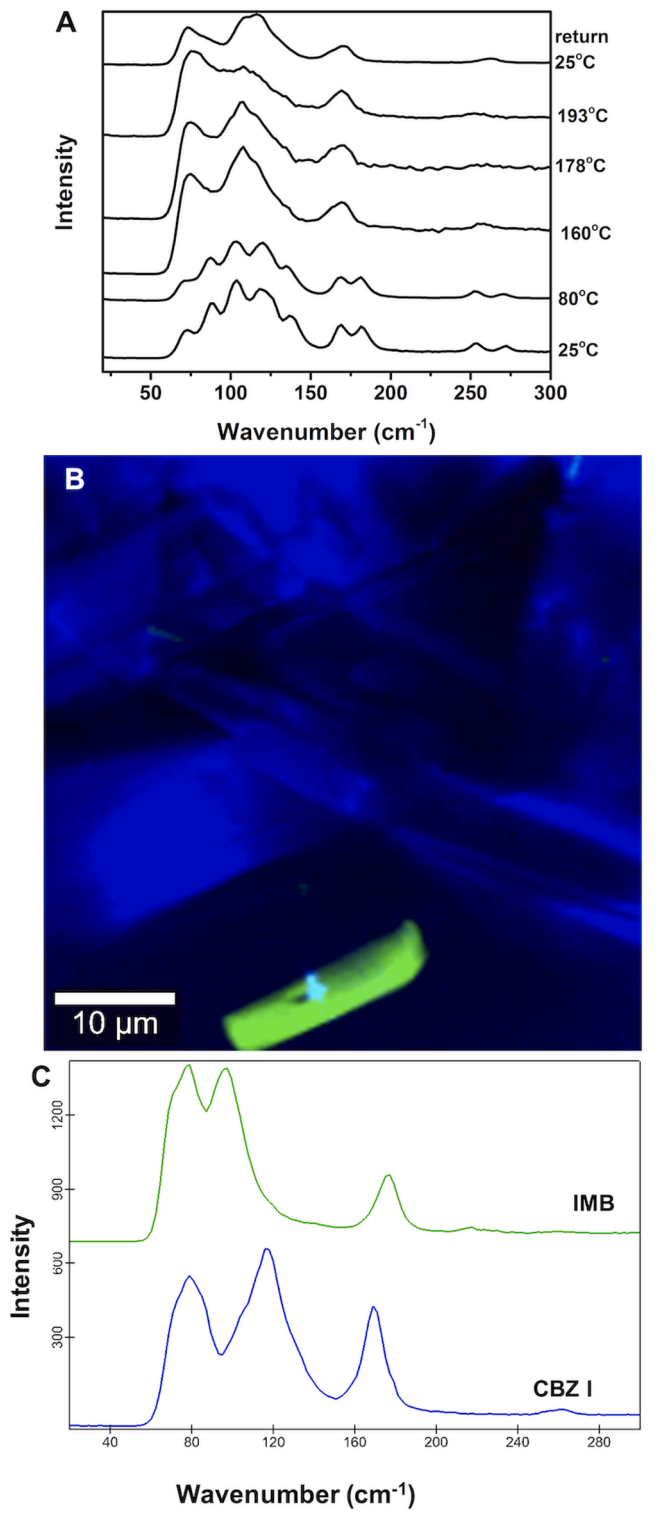

Fig. 10. A) Temperature-dependent Raman spectra for CBZ **III**. B) Combined Raman image showing the presence of CBZ I (blue) and IMS (green) particles in the final powder after cooling to room temperature. C) Raman spectra (colors as in image B) used for the combined Raman image, obtained by CA. (For interpretation of the references to colour in this figure legend, the reader is referred to the web version of this article.)

We propose as a new explanation for observing a distinct Raman spectrum in selected areas of the CBZ **III** sample, the existence of distinct crystallographic ordering in the molecular packing of carbamazepine. (Flicker et al., 2011; Krahn and Mielck, 1989) We have also observed differences in the relative intensities of the peaks (14.9°, 18° and 27.2°) in the XRD diffractogram of CBZ **III** (Fig. 8), which is in line with this hypothesis. According to Krahn and Mielck, CBZ **I** shows a similar behavior because depending on the synthesis method, a different crystallographic ordering is observed.(Krahn and Mielck, 1989) In order to further confirm this hypothesis, we have prepared pure CBZ **III** using the method proposed by Li *et al.*, (Li et al., 2008) and the same behavior was observed. In the Raman image, two different Raman spectra were observed, one corresponding to CBZ **III** and other similar to the Raman spectrum presented in Fig. 4B (data not shown). This result corroborates the idea that the commercial sample of CBZ **III** can exhibit different crystallographic ordering, which might result in distinct spectra as detected by confocal Raman microscopy, and not necessarily associated with the existence of other polymorph or chemical impurities.

According to Dołęga *et al.*,(Dołęga et al., 2020a, 2020b, 2019) the behavior of CBZ **III** upon heating the sample near the melting temperature of CBZ **I** (~192°) has been less studied. So, Raman imaging was used to study the polymorphic transition of CBZ **III** into CBZ **I** after cooling or re-heating CBZ **III** sample. The DSC analysis coupled with Raman imaging demonstrated that the CBZ **III** crystallized into CBZ **I** needle-shaped crystals and degraded into IMS particles after two heating–cooling cycles at a slow heating rate (5 °C/min) (Fig. 6). For CBZ **I** powder, the presence of IMS was also found in the final product (Fig. 7). The powder XRD for CBZ **III** recorded in function of temperature, up to 178 °C for 5 min, converted into CBZ **I** due to the appearance of the characteristic diffraction peaks of the triclinic form (Fig. 9). The Raman imaging analysis found a mixture of CBZ **III** and CBZ **I** on the final powder at room temperature, being the latter in more abundance on the sample. In this experiment, no evidence of IMS formation was observed.

It should be noticed that this result is different from the result obtained using the DSC technique, in which all CBZ **III** powder melted and recrystallized into CBZ **I** at 178 °C (Fig. 7, fist heating cycle). Moreover, the DSC analysis of CBZ **III** using only one heating–cooling cycle at 173 °C, followed by Raman imaging, demonstrates that all CBZ **III** crystallized into CBZ **I** (Figure S8). In this case, the Raman images did not show CBZ **III** or IMS residues. By extending the heating step to 193 °C using the XRD, the total conversion of CBZ **III** into CBZ **I** occurs as monitored by the Raman images without IMS residues present (Figure S4).

The Raman spectroscopy with variable temperature, followed by Raman imaging, allow to withdraw similar conclusions to the ones obtained with the DSC. In this case, the CBZ **III** starts to crystallize into CBZ **I** at 160 °C and at higher temperature (193 °C) it seems that all the CBZ **III** was converted into CBZ **I**; but a careful look at the sample using Raman imaging after cooling to room temperature, allowed to detect a mixture of CBZ **I** and IMS. A plausible explanation for this behavior is the type of environment in which the sample is submitted. For example, in the DSC measurements, the CBZ samples were placed in a hermetically closed pan, while the temperature-dependent Raman spectroscopy analysis was performed in a CBZ **III** sample between two glass slides. In both analyses, a mixture of CBZ **I** and IMS was obtained in the final powder after treatment at a temperature near the melting point of CBZ **I** (193 °C). It has been reported that the sublimation of IMS can occur at this temperature.(Dołęga et al., 2021, 2020b, 2020b) Dołęga *et al.* have demonstrated that IMS can sublimate at temperatures a dozen degrees of Celsius lower than its melting point (200 °C).(Dołęga et al., 2021)

On the other hand, the temperature-dependent powder XRD used non-closed sample holders, in which the evaporation of IMS and isocyanic acid (a second product of CBZ decomposition) from the system can occur, even at lower amounts. Thus, the degradation of CBZ samples can actually occur but not be observed by Raman imaging. Dołęga *et al.* have demonstrated the absence of IMS in DSC measurements of CBZ hydrate when a hermetically closed pan with a punctured lid is used. They have concluded that the IMS is formed and dissipated through the open systems.(Dołęga et al., 2020b)

5. Conclusions

In conclusion, our results reveal that not only the temperature influences the polymorph transition and degradation of CBZ, but also its detection is influenced by practical aspects used in each technique, such as a sealed or open sampler older. Raman imaging plays a vital role in monitoring the crystallization of CBZ **III** into CBZ **I** and identifying its degradation by the presence of IMS residues, even at lower amount, after being exposed to variable temperatures. Both CBZ polymorphs present a mixture of CBZ **I** crystals and IMS particles when exposed to higher temperatures in a closed system; however, only CBZ **I** crystals were observed in an open system (Powder XRD).

Raman imaging with CA provides a sensitive methodology to monitor polymorphic transitions/degradation products and could be used to perform quality control in final products, namely pharmaceutical formulations.

Authors contributions

Sara Fateixa: Research planning, Methodology, Writing-original draft preparation. **Helena I.S. Nogueira:** Writing- Reviewing and Editing. **Tito Trindade:** General scientific guidance, Writing- reviewing and editing.

Declaration of Competing Interest

The authors declare that they have no known competing financial interests or personal relationships that could have appeared to influence the work reported in this paper.

Acknowledgement

This work was developed within the scope of the project CICECO-Aveiro Institute of Materials, UIDB/50011/2020 & UIDP/50011/2020, financed by national funds through the FCT/MEC and when appropriate cofinanced by FEDER under the PT2020 Partnership Agreement. S. F. thanks FCT for his research contract (REF-069-88-ARH-2018) which is funded by national funds (OE), through FCT-Fundação para a Ciência e aTecnologia, I.P., in the scope of the framework contract foreseen in the numbers 4, 5, and 6 of the article 23, of the Decree-Law 57/2016, of August 29, changed by Law 57/2017, of July 19.

Appendix A. Supplementary material

Supplementary data to this article can be found online at https://doi.org/10.1016/j.ijpharm.2022.121632.

References

Arlin, J.-B., Price, L.S., Price, S.L., Florence, A.J., 2011. A strategy for producing predicted polymorphs: catemeric carbamazepine form V. Chem. Commun. 47, 7074–7076. https://doi.org/10.1039/C1CC11634G.

Bechtloff, B., Nordhoff, S., Ulrich, J., 2001. Pseudopolymorphs in Industrial Use. Cryst. Res. Technol. 36, 1315–1328. https://doi.org/10.1002/1521-4079(200112)36:12<1315::aid-crat1315>3.0.co;2-r.

Behme, R.J., Brooke, D., 1991. Heat of fusion measurement of a low melting polymorph of carbamazepine that undergoes multiple-phase changes during differential scanning calorimetry analysis. J. Pharm. Sci. 80 (10), 986–990. https://doi.org/10.1002/jps.2600801016.

Brown, S.C., Claybourn, M., Sievwright, D., Fearnside, V., Ashman, C., 2010. Lean Raman imaging for rapid assessment of homogeneity in pharmaceutical formulations. Appl. Spectrosc. 64 (4), 442–447. https://doi.org/10.1366/000370210791114239.

Carruthers, H., Clark, D., Clarke, F., Faulds, K., Graham, D., 2021. Comparison of Raman and near-infrared chemical mapping for the analysis of pharmaceutical tablets. Appl. Spectrosc. 75 (2), 178–188.

Censi, R., Di Martino, P., 2015. Polymorph impact on the bioavailability and stability of poorly soluble drugs. Molecules 20 (10), 18759–18776.

Ceolin, R., Toscani, S., Gardette, M.-F., Agafonov, V.N., Dzyabchenko, A.V., Bachet, B., 1997. X-ray Characterization of the Triclinic Polymorph of Carbamazepine. J. Pharm. Sci. 86, 1062–1065, 10.1021/js960338k.

Chemical Characterization of Pharmaceutical Samples by Confocal Raman Microscopy and Correlative Techniques [WWW Document], n.d. URL www.WITec.de (accessed 2.25.22).

Clarke, F.C., Jamieson, M.J., Clark, D.A., Hammond, S.V., Jee, R.D., Moffat, A.C., 2001. Chemical Image Fusion. The Synergy of FT-NIR and Raman Mapping Microscopy To Enable a More Complete Visualization of Pharmaceutical Formulations. Anal. Chem. 73 (10), 2213–2220. https://doi.org/10.1021/ac0013271.

Clout, A.E., Buanz, A.B.M., Gaisford, S., Williams, G.R., 2018. Polymorphic Phase Transitions in Carbamazepine and 10,11-Dihydrocarbamazepine. Chemistry 24 (51), 13573–13581. https://doi.org/10.1002/chem.201802368.

Dadou, S.M., El-Barghouthi, M.I., Antonijevic, M.D., Chowdhry, B.Z., Badwan, A.A., 2020. Elucidation of the Controlled-Release Behavior of Metoprolol Succinate from Directly Compressed Xanthan Gum/Chitosan Polymers: Computational and Experimental Studies. ACS Biomater. Sci. Eng. 6 (1), 21–37. https://doi.org/10.1021/acsbiomaterials.8b01028.

Di Febo, R., Casas, L., del Campo, Á.A., Rius, J., Vallcorba, O., Melgarejo, J.C., Capelli, C., 2020. Recognizing and understanding silica-polymorph microcrystals in ceramic glazes. J. Eur. Ceram. Soc. 40, 6188–6199, 10.1016/j.jeurceramsoc.2020.05.063.

Diao, Y., Whaley, K.E., Helgeson, M.E., Woldeyes, M.A., Doyle, P.S., Myerson, A.S., Hatton, T.A., Trout, B.L., 2012. Gel-Induced Selective Crystallization of Polymorphs. J. Am. Chem. Soc. 134 (1), 673–684. https://doi.org/10.1021/ja210006t.

Dołęga, A., Juszyńska-Gałązka, E., Deptuch, A., Jaworska-Gołąb, T., Zieliński, P.M., 2021. Thermoanalytical studies of a cytotoxic derivative of carbamazepine: iminostilbene. J. Therm. Anal. Calorim. 146 (5), 2151–2160. https://doi.org/10.1007/s10973-020-10410-w.

Dołęga, A., Juszyńska-Gałązka, E., Deptuch, A., Jaworska-Gołąb, T., Zieliński, P.M., 2020a. Vibrational Dynamics of Carbamazepine: Studies Based on Two-Dimensional Correlation Spectroscopy and X-ray Diffraction. Appl. Spectrosc. 74 (4), 473–484. https://doi.org/10.1177/0003702819891621.

Dołęga, A., Krupa, A., Zieliński, P.M., 2020b. Enhanced thermal stability of carbamazepine obtained by fast heating, hydration and re-crystallization from organic solvent solutions: A DSC and HPLC study. Thermochim. Acta 690, 178691. https://doi.org/10.1016/j.tca.2020.178691.

Dołęga, A., Zieliński, P.M., Osiecka-Drewniak, N., 2019. New Insight Into Thermodynamical Stability of Carbamazepine. J. Pharm. Sci. 108, 2654–2660, 10.1016/j.xphs.2019.03.027.

Edwards, A.D., Shekunov, B.Y., Forbes, R.T., Grossmann, J.G., York, P., 2001. Time-resolved x-ray scattering using synchrotron radiation applied to the study of a polymorphic transition in carbamazepine. J. Pharm. Sci. 90 (8), 1106–1114. https://doi.org/10.1002/jps.1064.

Farias, M., Carneiro, R., 2014. Simultaneous quantification of three polymorphic forms of carbamazepine in the presence of excipients using Raman spectroscopy. Molecules 19, 14128–14138. https://doi.org/10.3390/molecules190914128.

Fateixa, S., Carvalho, R.S., Daniel-da-Silva, A.L., Nogueira, H.I.S., Trindade, T., 2017. Luminescent Carrageenan Hydrogels Containing Lanthanopolyoxometalates. Eur. J. Inorg. Chem. 2017 (43), 4976–4981. https://doi.org/10.1002/ejic.201700888.

Fateixa, S., Nogueira, H.I.S., Trindade, T., 2018a. Surface-Enhanced Raman Scattering Spectral Imaging for the Attomolar Range Detection of Crystal Violet in Contaminated Water. ACS Omega 3 (4), 4331–4341. https://doi.org/10.1021/acsomega.7b0198310.1021/acsomega.7b01983.s001.

Fateixa, S., Raposo, M., Nogueira, H.I.S., Trindade, T., 2018b. A general strategy to prepare SERS active filter membranes for extraction and detection of pesticides in water. Talanta 182, 558–566, 10.1016/j.talanta.2018.02.014.

Firkala, T., Farkas, A., Vajna, B., Farkas, I., Marosi, G., 2013. Investigation of drug distribution in tablets using surface enhanced Raman chemical imaging. J. Pharm. Biomed. Anal. 76, 145–151, 10.1016/j.jpba.2012.12.017.

Flicker, F., Eberle, V.A., Betz, G., 2012. Recrystallization of commercial carbamazepine samples-a strategy to control dissolution variability. Pharmaceutics 4, 58–70. https://doi.org/10.3390/pharmaceutics4010058.

Flicker, F., Eberle, V.A., Betz, G., 2011. Variability in commercial carbamazepine samples–impact on drug release. Int. J. Pharm. 410 (1-2), 99–106. https://doi.org/10.1016/j.ijpharm.2011.03.032.

Grzesiak, A.L., Lang, M., Kim, K., Matzger, A.J., 2003. Comparison of the Four Anhydrous Polymorphs of Carbamazepine and the Crystal Structure of Form I. J. Pharm. Sci. 92, 2260–2271, 10.1002/jps.10455.

Hilfiker, R., 2006. Polymorphism: in the Pharmaceutical Industry. WILEY-VCH Verlag GmbH & Co, Weinheim.

Hilfiker, R., Raumer, M.v., 2019. Polymorphism in the Pharmaceutical Industry: Solid Form and Drug Development. Wiley-VCH Verlag GmbH & Co, KGaA, Weinheim, Germany.

Hu, C., Testa, C.J., Shores, B.T., Wu, W., Shvedova, K., Born, S.C., Chattopadhyay, S., Takizawa, B., Mascia, S., 2019a. An experimental study on polymorph control andcontinuous heterogeneous crystallization ofcarbamazepine. CrysEngComm 21 (34), 5076–5083.

Hu, C., Testa, C.J., Shores, B.T., Wu, W., Shvedova, K., Born, S.C., Chattopadhyay, S., Takizawa, B., Mascia, S., 2019b. An experimental study on polymorph control andcontinuous heterogeneous crystallization of carbamazepine. CrysEngComm 21 (34), 5076–5083.

Inoue, M., Hisada, H., Koide, T., Carriere, J., Heyler, R., Fukami, T., 2017. In Situ Monitoring of Crystalline Transformation of Carbamazepine Using Probe-Type Low-Frequency Raman Spectroscopy. Org. Process Res. Dev. 21 (2), 262–265. https://doi.org/10.1021/acs.oprd.6b0032910.1021/acs.oprd.6b00329.s001.

Inoue, M., Hisada, H., Koide, T., Fukami, T., Roy, A., Carriere, J., Heyler, R., 2019. Transmission Low-Frequency Raman Spectroscopy for Quantification of Crystalline

Polymorphs in Pharmaceutical Tablets. Anal. Chem. 91 (3), 1997–2003. https://doi.org/10.1021/acs.analchem.8b0436510.1021/acs.analchem.8b04365.s001.
Kipouros, K., Kachrimanis, K., Nikolakakis, I., Malamataris, S., 2005. Quantitative analysis of less soluble form IV in commercial carbamazepine (form III) by diffuse reflectance fourier transform spectroscopy (DRIFTS) and lazy learning algorithm. Anal. Chim. Acta 550, 191–198, 10.1016/j.aca.2005.06.063.
Kobayashi, Y., Ito, S., Itai, S., Yamamoto, K., 2000. Physicochemical properties and bioavailability of carbamazepine polymorphs and dihydrate. Int. J. Pharm. 193, 137–146, 10.1016/S0378-5173(99)00315-4.
Kogermann, K., Aaltonen, J., Strachan, C.J., Pöllänen, K., Veski, P., Heinämäki, J., Yliruusi, J., Rantanen, J., 2007. Qualitative in situ analysis of multiple solid-state forms using spectroscopy and partial least squares discriminant modeling. J. Pharm. Sci. 96 (7), 1802–1820. https://doi.org/10.1002/jps.20840.
Krahn, F.U., Mielck, J.B., 1989. Effect of type and extent of crystalline order on chemical and physical stability of carbamazepine. Int. J. Pharm. 53 (1), 25–34. https://doi.org/10.1016/0378-5173(89)90357-8.
Kuramshina, G.M., Mogi, T., Takahashi, H., 2003. Structures and vibrational spectra of 5H-dibenz[b, f]azepine and 5H-dibenzo[a, d]cycloheptene-5-ol on the basis of quantum mechanical calculations. J. Mol. Struct. 661–662, 121–139. https://doi.org/10.1016/j.molstruc.2003.07.016.
Lang, M., Kampf, J.W., Matzger, A.J., 2002. Form IV of Carbamazepine. J. Pharm. Sci. 91, 1186–1190, 10.1002/jps.10093.
Larkin, P.J., Dabros, M., Sarsfield, B., Chan, E., Carriere, J.T., Smith, B.C., 2014. Polymorph Characterization of Active Pharmaceutical Ingredients (APIs) Using Low-Frequency Raman Spectroscopy. Appl. Spectrosc. 68 (7), 758–776. https://doi.org/10.1366/13-07329.
Li, J., Qin, J., Zhang, X.u., Wang, R., Liang, Z., He, Q., Wang, Z., Wang, K., Wang, S., 2019. Label-free Raman imaging of live osteosarcoma cells with multivariate analysis. Appl. Microb. CELL Physiol. 103 (16), 6759–6769. https://doi.org/10.1007/s00253-019-09952-3.
Li, Y.i., Chow, P.S., Tan, R.B.H., Black, S.N., 2008. Effect of Water Activity on the Transformation between Hydrate and Anhydrate of Carbamazepine. Org. Process Res. Dev. 12 (2), 264–270. https://doi.org/10.1021/op7001497.
Marques, C.F., Olhero, S.M., Torres, P.M.C., Abrantes, J.C.C., Fateixa, S., Nogueira, H.I. S., Ribeiro, I.A.C., Bettencourt, A., Sousa, A., Granja, P.L., Ferreira, J.M.F., 2019. Novel sintering-free scaffolds obtained by additive manufacturing for concurrent bone regeneration and drug delivery: Proof of concept. Mater. Sci. Eng. C 94, 426–436, 10.1016/j.msec.2018.09.050.
Meyer, M.C., Straughn, A.B., Jarvi, E.J., Wood, G.C., Pelsor, F.R., Shah, V.P., 1992. The Bioinequivalence of Carbamazepine Tablets with a History of Clinical Failures. Pharm Res 9, 1612–1616. https://doi.org/10.1023/a:1015872626887.
Mitsutake, H., Poppi, R.J., Breitkreitz, M.C., 2019. Raman Imaging Spectroscopy: History, Fundamentals and Current Scenario of the Technique. J. Braz. Chem. Soc. 30, 2243–2258.
Mittapalli, P.K., Suresh, B., Hussaini, S.S.Q., Rao, Y.M., Apte, S., 2008. Comparative in vitro study of six carbamazepine products. AAPS PharmSciTech 9 (2), 357–365. https://doi.org/10.1208/s12249-008-9035-y.
Monteiro, A.R., Ramos, C.I.V., Fateixa, S., Moura, N.M.M., Neves, M.G.P.M.S., Trindade, T., 2018. Hybrids Based on Graphene Oxide and Porphyrin as Tools for Detection and Stabilization of DNA G-Quadruplexes. ACS Omega 3 (9), 11184–11191. https://doi.org/10.1021/acsomega.8b0136610.1021/acsomega.8b01366.s001.
Nanubolu, J.B., Burley, J.C., 2012. Investigating the Recrystallization Behavior of Amorphous Paracetamol by Variable Temperature Raman Studies and Surface Raman Mapping. Mol. Pharm. 9 (6), 1544–1558. https://doi.org/10.1021/mp300035g.
O'Brien, L.E., Timmins, P., Williams, A.C., York, P., 2004. Use of in situ FT-Raman spectroscopy to study the kinetics of the transformation of carbamazepine polymorphs. J. Pharm. Biomed. Anal. 36, 335–340, 10.1016/j.jpba.2004.06.024.
Piqueras, S., Duponchel, L., Tauler, R., de Juan, A., 2014. Monitoring polymorphic transformations by using in situ Raman hyperspectral imaging and image multiset analysis. Anal. Chim. Acta 819, 15–25, 10.1016/j.aca.2014.02.027.
Prasad, R., Panwar, K., Katla, J., Dalvi, S.V., 2020. Polymorphism and Particle Formation Pathway of Carbamazepine during Sonoprecipitation from Ionic Liquid Solutions. Cryst. Growth Des. 20 (8), 5169–5183. https://doi.org/10.1021/acs.cgd.0c0038210.1021/acs.cgd.0c00382.s001.
Rocha, W.F. de C., Poppi, R.J., 2011. Multivariate control charts based on net analyte signal (NAS) and Raman spectroscopy for quality control of carbamazepine. Anal. Chim. Acta 705, 35–40. https://doi.org/10.1016/j.aca.2011.03.024.
Rodriguez-Spong, B., Price, C.P., Jayasankar, A., Matzger, A.J., Rodriguez-Hornedo, N., 2004. General principles of pharmaceutical solid polymorphism: A supramolecular perspective. Adv. Drug Deliv. Rev. 56, 241–274. https://doi.org/10.1016/j.addr.2003.10.005.
Roy, S., Chamberlin, B., Matzger, A.J., 2013. Polymorph Discrimination Using Low Wavenumber Raman Spectroscopy. Org. Process Res. Dev. 17 (7), 976–980. https://doi.org/10.1021/op400102e.
Rustichelli, C., Gamberini, G., Ferioli, V., Gamberini, M.C., Ficarra, R., Tommasini, S., 2000a. Solid-state study of polymorphic drugs: Carbamazepine, in. Journal of Pharmaceutical and Biomedical Analysis. Elsevier 23 (1), 41–54. https://doi.org/10.1016/S0731-7085(00)00262-4.
Rustichelli, C., Gamberini, G., Ferioli, V., Gamberini, M.C., Ficarra, R., Tommasini, S., 2000b. Solid-state study of polymorphic drugs: carbamazepine. J. Pharm. Biomed. Anal. 23, 41–54, 10.1016/S0731-7085(00)00262-4.
Sarri, B., Canonge, R., Audier, X., Lavastre, V., Pénarier, G., Alie, J., Rigneault, H., 2019. Discriminating polymorph distributions in pharmaceutical tablets using stimulated Raman scattering microscopy. J. Raman Spectrosc. 50 (12), 1896–1904. https://doi.org/10.1002/jrs.5743.
Środek, D., Dulski, M., Galuskina, I., 2018. Raman imaging as a new approach to identification of the mayenite group minerals. Sci. Rep. 8 (1) https://doi.org/10.1038/s41598-018-31809-4.
Strachan, C.J., Howell, S.L., Rades, T., Gordon, K.C., 2004a. A theoretical and spectroscopic study of carbamazepine polymorphs. J. Raman Spectrosc. 35 (5), 401–408. https://doi.org/10.1002/jrs.1134.
Strachan, C.J., Pratiwi, D., Gordon, K.C., Rades, T., 2004b. Quantitative analysis of polymorphic mixtures of carbamazepine by Raman spectroscopy and principal components analysis. J. Raman Spectrosc. 35 (5), 347–352. https://doi.org/10.1002/jrs.1140.
Taylor, L.S., Zografi, G., 1998. The Quantitative Analysis of Crystallinity Using FT-Raman Spectroscopy. Pharm Res 15, 755–761. https://doi.org/10.1023/a:1011979221685.
Tian, F., Zeitler, J.A., Strachan, C.J., Saville, D.J., Gordon, K.C., Rades, T., 2006. Characterizing the conversion kinetics of carbamazepine polymorphs to the dihydrate in aqueous suspension using Raman spectroscopy. J. Pharm. Biomed. Anal. 40, 271–280, 10.1016/j.jpba.2005.07.030.
Tommasini, M., Zanchi, C., Lucotti, A., Bombelli, A., Villa, N.S., Casazza, M., Ciusani, E., de Grazia, U., Santoro, M., Fazio, E., Neri, F., Trusso, S., Ossi, P.M., 2019. Laser-Synthesized SERS Substrates as Sensors toward Therapeutic Drug Monitoring. Nanomaterials 9 (5), 677. https://doi.org/10.3390/nano9050677.
Xu, T., Yilmaz, H., Willett, D.R., Strasinger, C., Rodriguez, J.D., Keire, D.A., Wokovich, A. M., 2020. Raman mapping of fentanyl transdermal delivery systems with off-label modifications. Analyst 145 (3), 953–962. https://doi.org/10.1039/C9AN01289C.